Strojniški vestnik - Journal of Mechanical Engineering 68(2022)1, 3-13
DOI:10.5545/sv-jme.2021.7329
Original Scientific Paper
Received for review: 2021-07-14
Received revised form: 2021-09-29
Accepted for publication: 2021-12-16


# Incorporation of a Simplified Mechanical Joint Model into Numerical Analysis

Mitja Glavan[1] – Jernej Klemenc[2] – Vili Malnarič[1] – Domen Šeruga[2,*]
[1] TPV Automotive, Slovenia
[2] University of Ljubljana, Faculty of Mechanical Engineering, Slovenia

*In the development of new joining technologies, incorporation of mechanical joints in computer analyses for the evaluation of structures can be carried out by a practical, simplified mechanical joint model. Here, two most frequently used joining technologies were analysed, a self-piercing rivet joint and a clinch joint. Physical tests of static load capacity of the joints were performed and numerical models for simulations were set-up. An optimization method was designed for estimating the material parameters of the mechanical joint for the needs of numerical analyses. For optimization purposes during the plan of experiments, a range of possible parameter values was investigated using a response surface method, results of simulations, results of physical tests and a genetic algorithm. The results of simulations using the optimal values of the material parameters are comparable to the experimental observations for the both joints.*

**Keywords: mechanical joints, self-piercing riveting, clinch joint, FEM of mechanical joints, parameter optimization, simplified FE model, response surface, genetic algorithm**

**Highlights**
- *Numerical model for modelling a mechanical joint has been defined.*
- *Methodology of defining the properties of material parameters in numerical analysis has been developed.*
- *The material parameters of the mechanical joint for 2 mm thick S500MC material have been defined.*
- *The developed methodology is fast and easy to use and represents a universal tool for industrial needs.*

## 0 INTRODUCTION

The current trend in the automotive, aerospace, nautical and other similar industries is primarily a decrease in material consumption and indirectly a reduction in the mass of these means of transportation. In this respect, today, the so-called lightweight materials such as high-strength steel, aluminium, composite materials and the use of magnesium are increasingly emerging as construction materials **[1]** to **[3]**. However, due to the different properties of these materials their joining with the traditional welding process is not possible. Today, a large number of alternative joining technologies is emerging, or is already in use, to meet the growing need in joining such materials **[4]** to **[9]**. A review of such technologies and their use can be seen in **[10]** to **[12]**. A wide range of technologies is thus in use, each with its advantages and disadvantages. The use of a particular technology hence depends on the strength requirements of the finished product, materials, the possibility of integration into production facilities and prices. Two joining technologies have been compared in our research, which possess the appropriate characteristics to represent an alternative to spot-welding. Self-piercing riveting is a technology that provides adequate static strength, i.e. load-bearing capacity of the joint and a slightly higher dynamic strength in contrast to spot welding, while the advantage of the clinch joint is a significantly higher dynamic load-bearing capacity, with the loss of a significant proportion of static load capacity **[13]** to **[16]**. Table 1 presents the comparison of the above technologies **[17]**. However, for a proper consideration of these technologies in numerical analyses during the pre-development and development phases of a research and development (R&D) cycle, it is necessary to develop appropriate numerical models of these joints. Moreover, knowing the exact parameters of joints contributes to reducing development costs, shorter development time and optimization of geometry before the first prototype is manufactured **[18]**.

As numerical structural analyses are carried out way before the production of prototypes and their physical testing, accurate knowledge of material parameters of the joint plays a key role in the quality of the simulations. For example, Bouchard et al. **[19]** used an approach with exact modelling of the actual rivet, which produced encouraging results even in the local area around the joint. Thus, following this approach, the numerical results are well comparable to physical testing, but such a model is not suitable for large structures and serves more for the purpose of understanding what happens in the joint and its surroundings. The disadvantages of such an approach are time-consuming simulations and possible

*Corr. Author's Address: University of Ljubljana, Faculty of Mechanical Engineering, Slovenia, domen.seruga@fs.uni-lj.si

**Table 1.** *An overview and comparison of self-piercing riveting (SPR) technology and clinch joint technology (adapted from [17])*

| Property | SPR | Clinching |
|---|---|---|
| Positioning on boreholes | No | No |
| Joining different materials | Yes | Yes |
| Joining three or more boards | Good | Poor |
| Sealing joint | Yes | Yes |
| Corrosion resistance | Good | Good |
| Visuality of the joint | Good | Medium |
| Access with the tool | Bilateral | Bilateral |
| Energy consumption | Low | Low |
| Environmental impact | Small | Small |
| Dynamic Strength | Good | Medium |
| Cycle time | Short | Short |
| Price | High | Low |

computational difficulties. For use in large structures, a reliable simplified numerical model is needed. Today, commercial software tools already offer various integrated numerical models that can be used for simulation of mechanical joints. Such an approach was used by e.g., Porcaro et al. **[10]**, Yang et al. **[20]** or Kulawik and Wrobel **[21]**. Porcaro et al. **[10]** used a pre-set spot-weld model in LS-Dyna software, which joined the sheet metal with a simple line element that connected it on the sheet through contact conditions that ensured a transfer of forces and torques between the two sheets. The material parameters, which influenced the result of numerical analyses, were adjusted and modified iteratively by the researchers based on matching the results of simulations to the results of physical tests. In a similar way, Sommer and Maier **[22]** and Hanssen et al. **[23]**, who were dealing with this issue using a more complex approach, used a calibration method in combination with physical tests to define the necessary joint parameters. Sommer and Maier **[22]** compared both several different geometric models of connecting elements and several different material models. They built various combinations of both geometric and material models and compared the results of numerical analyses with physical testing at chosen load cases. The material parameters were estimated on the basis of the calibration process that was based on the numerical force-displacement curve fitting to the curve obtained from the test. The results were promising and proved a good match with the experimental observations. Similarly, Hanssen et al. **[23]** focused on a numerical model and developed an algorithm to identify parameters of a numerical model, again based on physical testing. According to this methodology, the user defines the point between the sheets where the riveted joint is located and defines the cross-section of that joint. The algorithm searches for all the relevant nodes in the cross-section area of the rivet and connects the sheet metal. Through these nodes the loads are transferred and the joint response is calculated by the algorithm. However, for the operation of the model and the algorithm, it is necessary to define a wide range of parameters, which must be estimated through physical testing in various load cases. Nevertheless, the results obtained from such a model match well with the actual state.

In this study, the mechanical joint has also been modelled in a simplified way, whilst the number of the necessary material parameters has been minimised to the lowest possible amount which still ensured comparable results of the simulations and experimental observations. This way a high computational efficiency for analyses of large structures can be preserved. Mechanical joints have been modelled with a line element that is connected to the two sheet metals. A bilinear material model has been assigned to both the sheet metal and the joint, as the results of physical tests show an extreme bilinearity until the point of failure. Nevertheless, the material parameters of the sheet metal and the joint have been separately considered in the simulations. Namely, the physical features of the joint have been incorporated into its bilinear behaviour. Thus, both the set and the range of the material parameters for the joint have first been defined. Next, using an optimization method based on the full factorial test and application of the response surface method in combination with a real-valued genetic algorithm, an optimal combination of the values of the material parameters has been determined. Finally, the numerical model of the mechanical joint for a 2 mm thick sheet metal of S500MC material has been validated.

## 1 METHODOLOGY

### 1.1 Experimental Set-up

Two types of joints of a 2 mm thick sheet metal made of S500MC material were tested, a self-piercing rivet joint and a clinch joint. Self-piercing rivets with diameter of 5 mm were manufactured and mechanical clinching tool with 8 mm diameter was used for clinch joints. Static tests have been performed on the joints during experimental validation.

Furthermore, two specimen types have been manufactured, the shapes of which were in compliance with the standard DVS/EFB 3480-1 **[24]**, see Fig. 1. The width of the specimens was 45 mm.

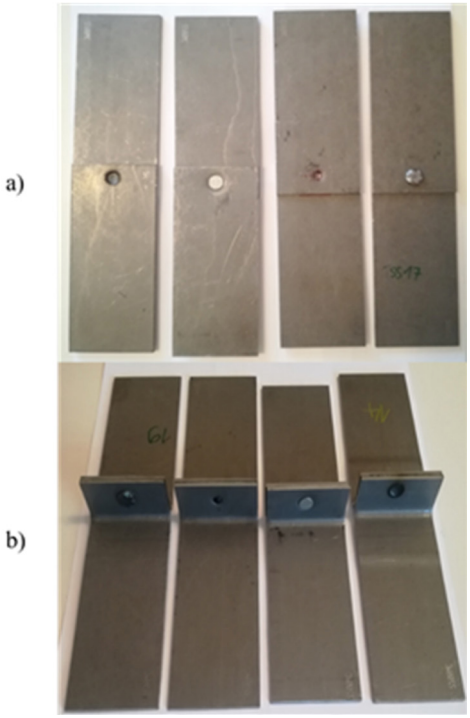


**Fig. 1.** *The specimens for physical tests: a) overlapping joint and b) flanged joint for peel tests*

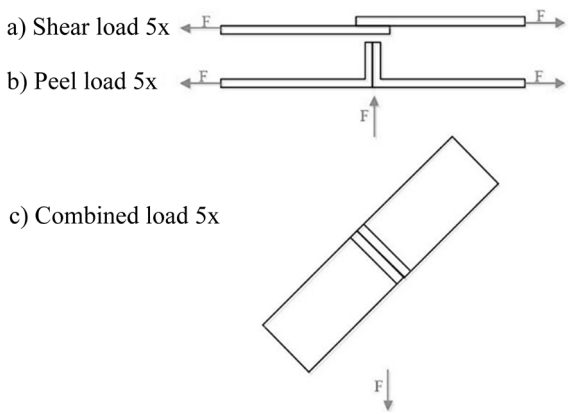


**Fig. 2.** *Loading conditions: a) for shear strength test; b) for the peel test; c) for the combined test; clamps of the test rig and the compensation tabs are pointed out during application of the combined load*

Specimen types corresponded to two load cases, which are also prescribed by the standard DVS/EFB 3480-1 **[24]**, and an additional combination of these two load cases, see Fig. 2:

- Static shear strength test for an overlapping joint.
- Static peel strength test for a flanged joint.
- Static combined tensile-shear test for a flanged joint, with a load at an angle of 45°. Additionally, compensation tabs to accommodate the misalignments of the specimens were adopted during the of tensile-shear test.

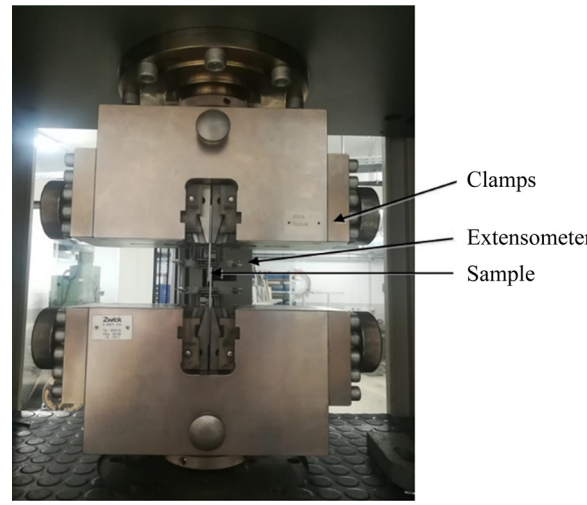


**Fig. 3.** *Layout of the test rig*

Each loading condition was repeated five times, for both types of joints. In total, 15 specimens for each type of the joint were tested. The tests were carried out on a certified Zwick/Roell Z150 test rig, see Fig. 3. The specimens were inserted in the clamps in the length of 40 mm. The load was applied by means of the clamp displacement at a rate of 10 mm/s with monitoring the force on the clamp at a given displacement. The results of each five repetitions were averaged, and the resulting force-displacement curve served as the basis for comparison with numerical simulations.

### 1.2 Numerical Model

Simulia Abaqus software was used to build the simplified finite-element model. The sheet metals were modelled with shell elements. The joint was modelled as a line connecting sheets by a kinematic or distributing connection as shown in Fig. 4. The size and the quality of the finite element mesh was generated according to the industrial requirements for crash simulations. Specifically, Timoshenko beams designated as B32 type in Abaqus were used to represent either the self-piercing rivet or the clinch joint. One beam connected the centres of the holes and several beams connected each centre of the hole with the circumferential nodes (Fig. 4).

A structured and denser mesh was created around the joint. Rectangular S4 type shell elements and triangular S3R type shell elements were applied. The size of the bore was equal to the diameter of the

connecting element representing the joint. A general contact was assigned between the sheets taking into account the friction between the sheets by a coefficient $\mu$ = 0.6 [25]. The boundary conditions represented the clamping of the sheets into the test rig. This involved fixed nodes on one sheet metal and application of prescribed displacement to the nodes on the other sheet metal to mimic the experimental setup as depicted in Fig. 2. The prescribed displacement was applied in a series of steps. The size of each step was limited upwards with 10 % of the final value of the displacement.

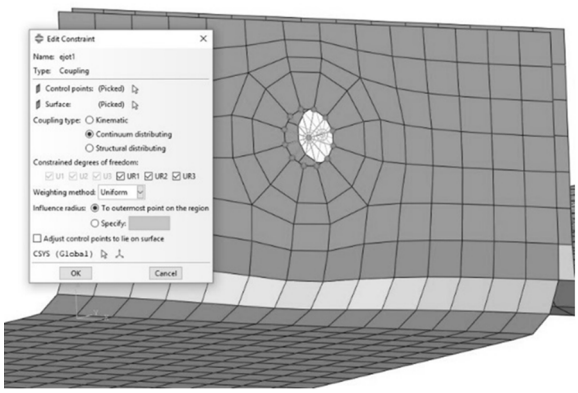


**Fig. 4.** *Model of the mechanical joint*

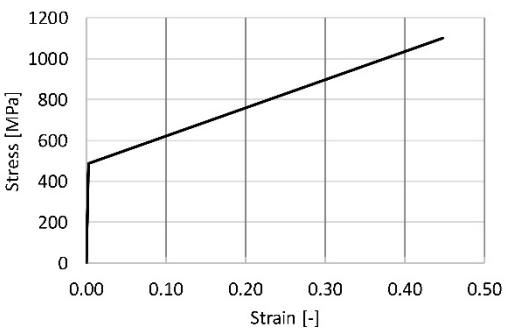


**Fig. 5.** *Bilinear true stress-strain curve used to model S500 MC sheet metal behaviour*

A bilinear true stress-strain curve for S500 MC is given in Fig. 5. The sheet metal was modelled using these properties. A bilinear material model and round cross-sections were also assigned to the line elements, which were used to model the joint. The diameter of the cross-section was equal to the cross-section of the connecting element. However, the parameters of the bilinear elastoplastic properties of the joint differed from the true material properties for S500 MC and rather represented its physical response under the loading. All the peculiarities of the joint were hence integrated and represented by the bilinear characteristic of the joint. The goal of the simulations was then to determine the optimal values of the parameters of the modelled joint. In doing so, a constant value of Poisson's ratio and a constant material density were assumed. Optimal values of the following parameters were searched for, which fully described the behaviour of the joint:

- elastic modulus, $E$ [MPa],
- tangent modulus, $E_T$ [MPa], and
- yield stress, $R_{p0.2}$ [MPa].

To define the optimal values of these parameters, a full factorial test was performed which used the response surface method in combination with genetic algorithm. In the first step, domain limits were defined within which the parameter values were searched for and these domains were then further divided into multiple values within the search area. In the next step, possible combinations $p$ of the parameter values were defined. For each of the combinations, a numerical analysis of the tensile test was then performed including each of the three load cases. In total, $3p$ simulations for each type of joint were performed. The numerically calculated force-displacement curves for each parameter combination and load case were compared to the experimental results. The agreement between the measured and the modelled response of a joint was then estimated using the sum of the squared distances (*SSQD*) for the force differences at a certain displacement:

$$SSQD^{(j)} = \sum_{i=1}^{K_j} (F_{\text{sim}}(x_i) - F_{\text{exp}}(x_i))^2, \quad (1)$$

where $F_{\text{exp}}$ represents the measured force from the tensile test, $F_{\text{sim}}$ is the calculated force as a result of numerical simulations, $j$ is the associated load case, $K_j$ is the number of repetitions of a load case, and $x$ represents the displacement. Since the main objective was to determine the material parameters that would optimally fit all three load cases, a multi-criteria objective function was defined as:

$$F_{\text{C}} = \sum_{j=1}^{n_{\text{T}}} w_j \cdot SSQD^{(j)}, \quad (2)$$

where $w_j$ represents a weight by which the significance or impact of each load case is attributed and $n_{\text{T}}$ stands for the number of load cases. For each combination of parameters defined in Table 2, the value of the objective function was calculated as:

$$F_{\text{C}}^{(m,n.o)} = F_{\text{C}}(E^{(m)}, E_{\text{T}}^{(n)}, R_{\text{p0.2}}^{(o)});$$
$$m = 1,...,k;\ n = 1,...,l;\ o = 1,...,r, \quad (3)$$

where $m$, $n$, and $o$ are the running indices through the levels of the material parameters, which are listed in Table 2. The most suitable values of the

material parameters are those that give the lowest value of the objective function $F_C$. The known values of combinations of parameters, together with the associated value of the objective function, represent the points in a four-dimensional space. These points are distributed relatively evenly throughout the space. Since the optimal combination of parameters lies within this range, it is not necessary for the optimal combination to be one of the combinations that were defined initially; the optimal combination might lie between the chosen points. Therefore, a response surface method was used, which enables an approximation of the surface through the calculated points in the four-dimensional space. This step then makes possible to determine the value of the objective function for any combination of material parameters, even for that combination which was not used during the numerical analysis.

The response surface for the objective function $F_C$ was modelled as the sum of global trend $F_{C,glob}$ and local specifics $F_{C,loc}$ of the objective function **[10]**, **[15]**, and **[26]**. The local deviations of the objective function from the global trend were modelled using a mixture of multivariate elliptical Gaussian functions whereas the whereas the global trend was modelled using a third-degree polynomial for the three independent variables ($E$, $E_T$ and $R_{p0.2}$) and one dependent variable (objective function $F_C$):

$$\begin{aligned} F_{\mathrm{C,glob}}(x_1,x_2,x_3) = a_0 &+ \sum_{r=1}^{3}\sum_{q=1}^{3} a_{r,q}x_q^r + a_{2,4}x_1x_2 \\ &+ a_{2,5}x_1x_3 + a_{2,6}x_2x_3 + a_{3,4}x_1^2x_2 \\ &+ a_{3,5}x_1x_2^2 + a_{3,6}x_1^2x_3 + a_{3,7}x_1x_3^2 \\ &+ a_{3,8}x_2^2x_3 + a_{3,9}x_2x_3^2 + a_{3,10}x_1x_2x_3, \end{aligned} \quad (4)$$

where:

$$x = \begin{bmatrix} x_1 \\ x_2 \\ x_3 \end{bmatrix} = \begin{bmatrix} E \\ E_T \\ R_{p0.2} \end{bmatrix}. \quad (5)$$

Parameters $a_0$ and $a_{r,q}$ are the parameters of the polynomials determined by the polynomial approximation for the $p$ points from Eq. (3). The coefficients of the polynomial were estimated from the experimental data using the pseudo-inverse matrix as follows:

$$\mathbf{a} = (\mathbf{X}^T \cdot \mathbf{X})^{-1} \cdot \mathbf{X}^T \cdot \mathbf{y}, \quad (6)$$

where the individual vectors and the matrix are the following:

$$\mathbf{a} = \begin{bmatrix} a_0 \\ a_{1,1} \\ \vdots \\ a_{3,10} \end{bmatrix}, \quad \mathbf{y} = \begin{bmatrix} F_C^{(1,1,1)} \\ F_C^{(1,1,2)} \\ \\ F_C^{(k,l,r)} \end{bmatrix},$$

$$\mathbf{x} = \begin{bmatrix} 1 & E^{(1)} & E_T^{(1)} & R_{p0.2}^{(1)} & \cdots & E^{(1)} & E_T^{(1)} & R_{p0.2}^{(1)} \\ 1 & E^{(1)} & E_T^{(1)} & R_{p0.2}^{(2)} & \cdots & E^{(1)} & E_T^{(1)} & R_{p0.2}^{(2)} \\ \vdots & \vdots & \vdots & \vdots & \ddots & \vdots & \vdots & \vdots \\ 1 & E^{(k)} & E_T^{(l)} & R_{p0.2}^{(r)} & \cdots & E^{(k)} & E_T^{(l)} & R_{p0.2}^{(r)} \end{bmatrix}. \quad (7)$$

The displacement points, in which the forces were compared, were selected based on the physical test results. As different load cases withstood different breakage forces at different final displacements, there was no possibility to choose exactly the same displacement points for all load cases. Based on the displacement-force diagram from the physical tests, the breakage point was established for each load case. This displacement was then used in numerical simulation as a maximum displacement by which the samples were loaded. The whole displacement range was divided equidistantly into 10 points, the final point being the breakage point from physical test. Those points were the displacement points in which the measured and the calculated forces were compared and used in Eq. (1).

Having determined the parameters of the polynomials that describe the global trend of the response surface, the residual $R_C$ between the actual value of the objective function $F_C$ and the value of its global trend of the $F_{C,glob}$ could be determined for each point from Eq. (3) as:

$$\begin{aligned} R_C^{(m,n,o)} &= F_C^{(m,n,o)} - F_{C,glob}^{(m,n,o)}, \\ m &= 1,\ldots,k, \quad n = 1,\ldots,l, \quad o = 1,\ldots,q. \end{aligned} \quad (8)$$

Then, the $R_C$ values were integrated into a conditional-average estimator using local multidimensional Gaussian functions to obtain a model of local specifics of the objective function $F_{C,loc}$ **[10]**, **[15]**, and **[25]**:

$$F_{C,loc} = \frac{\sum_{m=1}^{k}\sum_{n=1}^{l}\sum_{o=1}^{q} R_C^{(m,n,o)} \cdot W\left(X - X^{(m,n,o)}; \sum^{(m,n,o)}\right)}{\sum_{m=1}^{k}\sum_{n=1}^{l}\sum_{o=1}^{q} W\left(X - X^{(m,n,o)}; \sum^{(m,n,o)}\right)}, \quad (9)$$

where $R_C^{(m,n,o)}$ stands for residuals from Eq. (8), $\mathbf{x}$ are vectors from Eq. (5), $W$ represent multidimensional Gaussian functions with median values vector in points $\mathbf{x}^{(m,n,o)}$ and $\boldsymbol{\Sigma}^{(m,n,o)}$ are covariant matrices

of individual Gaussian functions. The individual multidimensional Gaussian functions $W$ were hence defined as:

$$W\left(\mathbf{x}-\mathbf{x}^{(m,n,o)};\Sigma^{(m,n,o)}\right)=\frac{\sqrt{\det\left[\left(\Sigma^{(m,n,o)}\right)^{-1}\right]}}{\left(2\cdot\pi\right)^{d/2}}$$

$$\cdot\exp\left[-\frac{1}{2}\cdot\left(\mathbf{x}-\mathbf{x}^{(m,n,o)}\right)^{\mathrm{T}}\cdot\left(\Sigma^{(m,n,o)}\right)^{-1}\cdot\left(\mathbf{x}-\mathbf{x}^{(m,n,o)}\right)\right],(10)$$

where $d$ is the dimension of the vector of independent variables, in this case the number of load cases ($d = 3$). Covariance matrices are diagonal with their variances equal to the distances to the nearest adjacent point in the direction of the individual components of vector **x**. In order to facilitate the data processing, individual variables (independent and dependent) were converted to logarithmic values before the process of global-local modelling of the objective function.

In the last step, the objective function surface was calculated and the response surface was defined:

$$\widehat{F}_{\mathrm{C}}(X)=F_{\mathrm{C,glob}}(X)+F_{\mathrm{C,loc}}(X). \qquad (11)$$

This way it was possible to model a multi-dimensional surface that arbitrarily approaches any actual value of the measured point or, in this case, the result of the numerical analysis for each combination of parameters, while maintaining the trend without local deviations even outside of the measurement range [18]. The response surface thus assists in finding the domain of the optimal parameter values, but it is still difficult to accurately determine the actual optimum. Here, a real-valued genetic algorithm was hence utilised, which enabled the determination of the optimal combination of material parameters of the joint, minimizing Eq. (11). The in-house genetic algorithm used in this study combined the classic single-point crossover and linear crossover. The mutation-with-momentum of the child chromosomes enabled a better fine-tuning of the later generations of chromosomes to the optimal solution [26] to [28]. A population size of $m$ = 20 randomly selected starting points on the response surface was used with the probability of crossover $p_{cr}$ = 0.5, fraction of linear crossover $f_{lin}$ = 0.6 and probability of mutation $p_{mut}$ = 0.05. The algorithm was stopped after 10000 generations which is usually sufficient for a satisfactory optimum [26]. The above-described procedure for determining the optimum values of the parameters $E$, $E_T$ and $R_{p0.2}$ was repeated for both joint types.


**Fig. 6.** *Broken-down specimens of: a) SPR joint, and b) clinch joint*

## 2 RESULTS

During the test, the force-displacement dependence was monitored and recorded until failure. In Fig. 6, the broken specimens are shown. The results of the measurements were filtered and represented in diagrams for all test repetitions of each load case, and then, based on the curves obtained, the average force-displacement curve was defined. This curve later served as the comparative indicator in the objective function. The average curve was generated to the point where the joint started to loosen and the value of the force began to decline, which is also seen in Figs. 7 and 8. The measurements showed good repeatability for both joint types and all three load cases. Only one of the results of the clinch joint measurements for the shear load case was later excluded as that specific measurement deviated incomparably from the other measurements. The final displacement of the average curve was also the displacement value up to which the numerical model of the joint was loaded.

Using the developed methodology, an optimal combination of the material parameters of the joint was generated, which on average can simulate the force-displacement responses best for all the three load cases, so they are hence suitable to use in a general model for any other load case. Additionally, the methodology was used to determine the material parameters considering only a single load case. This served for verification purposes and confirmation of

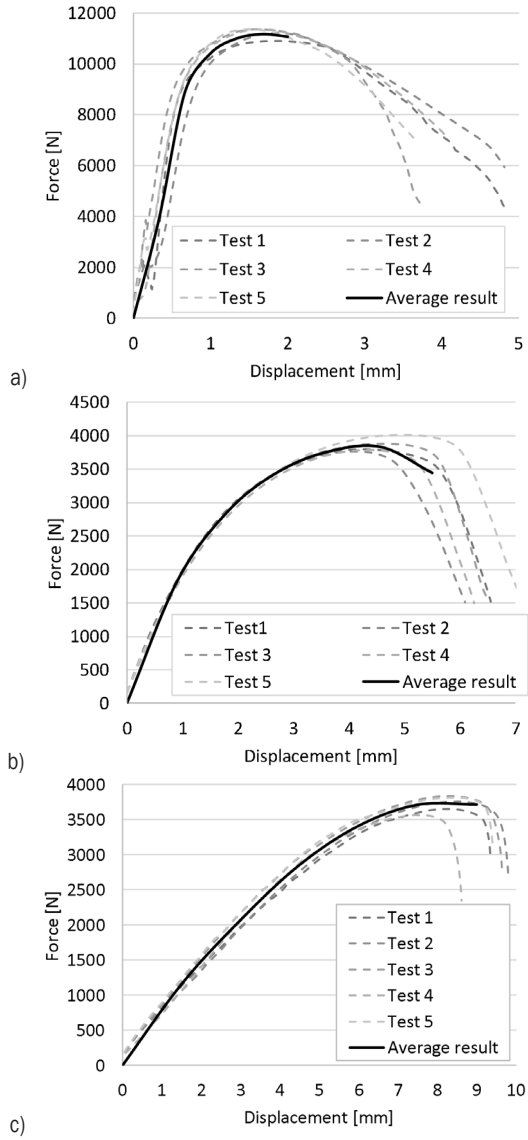


**Fig. 7.** *Measurement results for SPR joint: a) shear load case, b) peel load case, and c) combined load case*

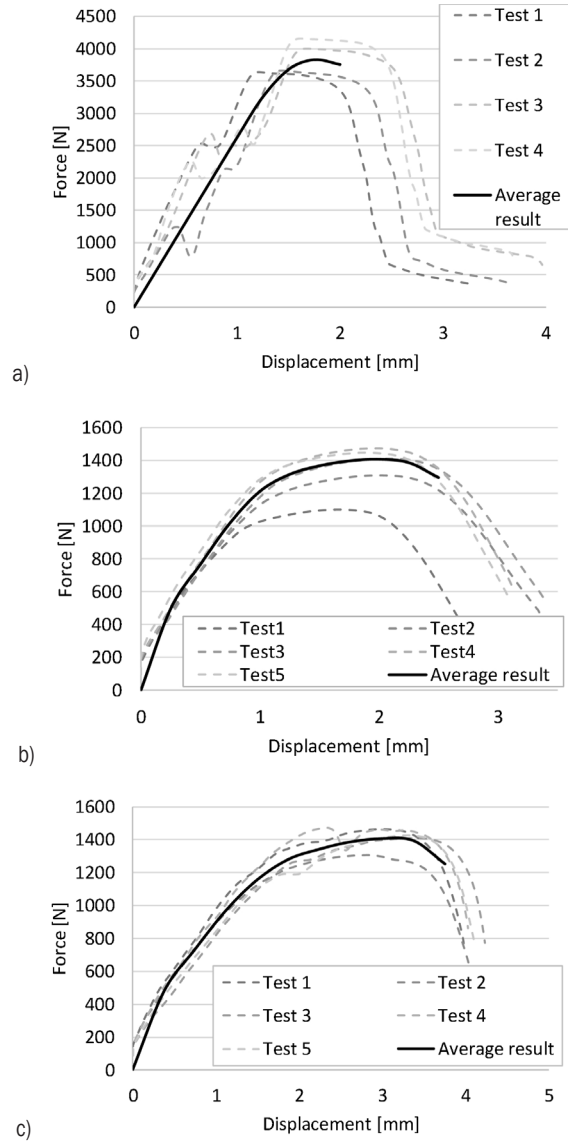


**Fig. 8.** *Measurement results for clinch joint: a) shear load case, b) peel load case and c) combined load case*

the best-fit ability of the method itself. During the parameter-estimation process, a starting point in the set of parameters was defined and a range of values within the algorithm performed its operation.

The range of values of the material parameters was divided approximately equidistantly in the logarithmic scale within the defined range. Table 2 shows the values and the range of parameters. In total, $p$ = 175 combinations of material parameters from Table 2 are possible for a single load case, which results in a total of $3p$ = 525 numerical analyses.

**Table 2.** *Values of parameters $E$ [MPa], $E_T$ [MPa] and $R_{p0.2}$ [MPa]*

| Parameter | Search domain | The values of the parameters taken into account | | | | | | |
|---|---|---|---|---|---|---|---|---|
| Elastic modulus - $E$ | 200-300000 | 200 | 500 | 1000 | 3000 | 10000 | 30000 | 300000 |
| Tangent modulus - $E_T$ | 0.1·E- 0.001·E | 0.1·E | 0.0286·E | | 0.01·E | 0.00286·E | | 0.001·E |
| Flow limit - $R_{p0.2}$ | 50-1000 | 50 | 100 | | 200 | 500 | | 1000 |

## 3 DISCUSSION

The force-displacement results of the measurements indicated that the response of each joint had a pronounced bilinear characteristic. Accordingly, the stress-strain behaviour of the connecting element in the joint was hence modelled using a bilinear material model. The failure of both the SPR and the clinch joint occurred in the very connection or in the connective element (Fig. 6). In the case of the SPR joint, the rivet was pulled out, and in the case of the clinch joint, the mechanical connection between the two sheets was broken. From this point of view, attention could be paid only to the connective element and its modelling, whilst the base material was modelled with a simple elastic-plastic material model.

It can be noted that in the case when each load case is treated separately (Figs. 9 and 10 – specific result), it is possible to accurately predict the combination of parameters that produce a numerical response of the joint almost identical to the measured response. By changing the range of the input parameters or even the type of the material model, a better agreement might also be possible to achieve. However, the method is primarily intended to determine the material parameters of the joints for general use in large structures with a large number of such joints whilst they are subjected to a random load. This response should therefore be the best approximation of the observed response of the joint regardless of the size and the direction of the applied load.

The method thus enables consideration of the agreement between the numerical and experimental response of the joint for several load cases. Consequently, the resulting values of the material parameters are always a compromise for several load cases and the deviation between the numerical response and the experimental response. A better agreement is hence always observed when only a single load case is considered during the estimation of the optimal material parameters.

Furthermore, other types of joints will have other properties therefore it is necessary to perform some initial tests under shear, peel and combined tensile-shear load conditions to be able to search for the optimal values of the parameters in the numerical model. After these have been performed however, the numerical model of a complex structure with such a joint can be used under arbitrary load conditions.

For the correct performance of the method, it is essential to correctly define the material model, the range of possible values of associated material parameters and to perform accurate measurements

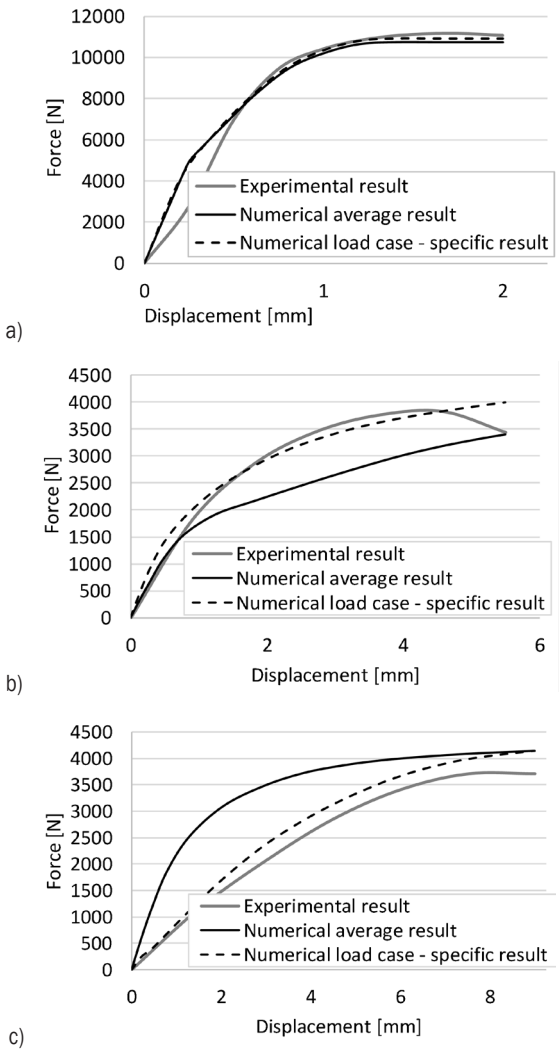


**Fig. 9.** *Comparison of numerical and actual response of SPR joint: a) shear load case, b) peel load case, c) combined load case*

which serve as a comparative value for numerical simulations. Choosing a more complex material model might lead to a more accurate understanding of the joint behaviour, while on the other hand, results in a more complex definition of the objective function and extends the numerical calculation time, which is of crucial importance in practice. Likewise, it is not possible to accurately determine the values of the material parameters if the search area is too wide or too narrow. If the search domain differs from the final area presented in Table 2, it may happen that the positions of the optimal parameter values lie outside of the defined search range. An example of such an inadequately defined search range is presented for the SPR joint in Fig. 11. The comparison of the results between the inadequately and adequately defined

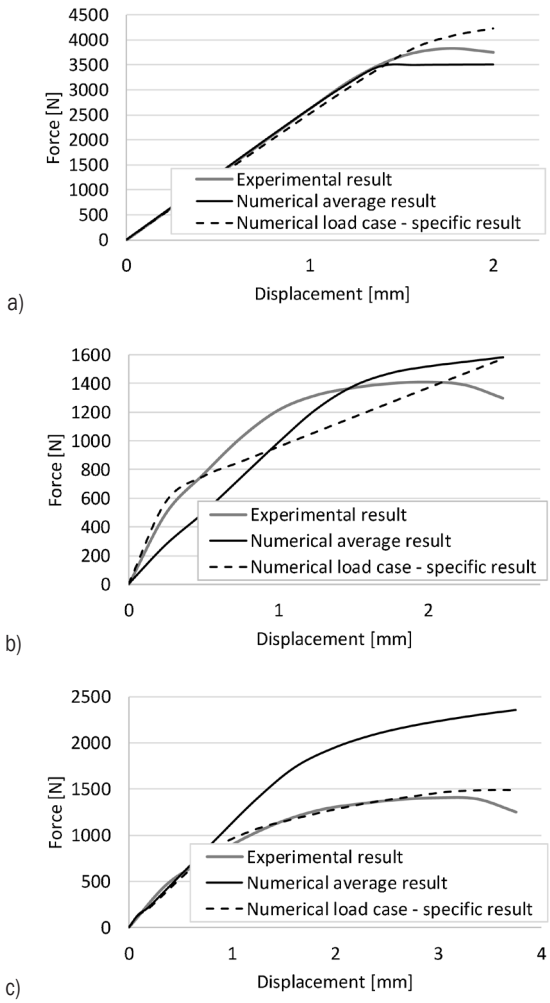


**Fig. 10.** *Comparison of numerical and actual clinch joint response: a) shear load case, b) peel load case, c) combined load case*

search ranges reveals that the force-displacement description can drastically differ if the initial search domain of the parameters is too wide.

The material model of the joint used in this study succeeds in describing the force-displacement response as long as the force increases with increasing displacement and shows a pronounced bilinearity. When the maximum force is achieved in practice, the joint begins to loosen, the force begins to decline, and the joint then gradually breaks down. In numerical analyses however, such behaviour of the joint cannot be modelled using a bilinear material model. Hence, only the "functional" part of the joint behaviour can be simulated, i.e., the increasing part of the force-displacement characteristics until the maximum force. For the correct performance of the developed methodology this fact has to be taken into account in numerical simulations so that the final simulated displacement coincides with the experimental displacement at the maximum value of the force. If the displacements exceeding this limit are considered during the optimization of the material parameters, the error of the method will increase as a consequence of the diverging experimental and simulated curves.

The final values of the material parameters can also be influenced by weights assigned to the load cases in the objective function. The importance of a specific load case can hence be considered. This is most easily explained if the values of forces that occur in individual load case are observed. The force in the case of the shear test is approximately twice as high as in the other load cases. Consequently, at higher force values, the relative difference of the numerical and the experimental result will be comparable to other load cases, whilst the absolute value of the difference will be significantly higher than for the other load cases.

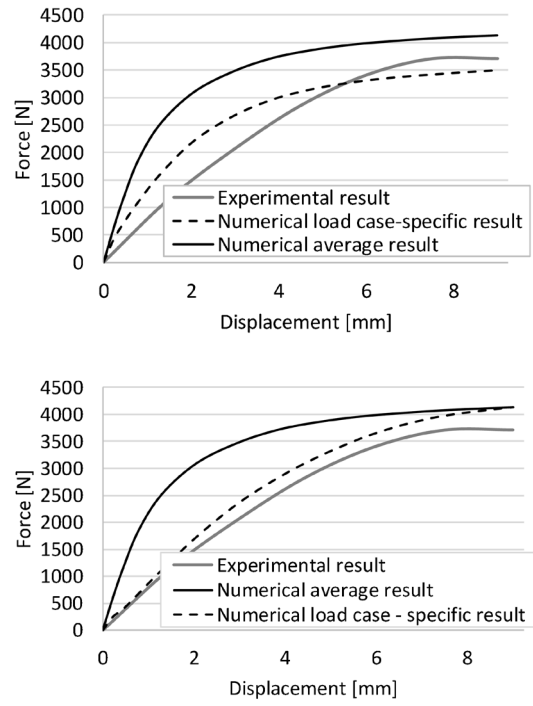


**Fig. 11.** *Force-displacement results for: a) inadequately defined search range, and b) adequately defined search range*

Hence, the value of the objective function strongly depends on the tensile case and less on the other two cases. Thus, by using weights, individual contributions of various load cases to the objective function can be balanced and their importance for the final result can be evenly distributed. Nevertheless, the above-mentioned differences did not provide a significant impact on the final result during this study,

therefore equal weights were attributed to the various load cases. The optimal values of the parameters to simulate the response of the self-piercing rivet joint were determined as $E$ = 8980 MPa, $E_T$ = 260 MPa and $R_{p0.2}$ = 217 MPa. Similarly, the optimal values of the parameters for the clinch joint were determined as $E$ = 1042 MPa, $E_T$ = 1.5 MPa and $R_{p0.2}$ = 195 MPa. Nevertheless, these values of the parameters represent synthetic properties of the joint and not the material properties of the assembly.

## 4 CONCLUSIONS

The force-displacement response of both the self-piercing rivet joint and the clinch joint tested during this study exhibited distinctly bilinear characteristics up to the highest measured force before failure. The presented methodology could be applied to determine optimal values of material parameters for the bilinear material model. Numerical analyses of large structures with a number of such joints, each having the same values of the material parameters, can thus be performed to simulate their stress-strain or force-displacement behaviour under variable loading. The optimal values of the material parameters represent a compromise between the quality of fit and the variety of load cases.

## 5 ACKNOWLEDGEMENTS

The authors acknowledge financial support from the Slovenian Research Agency (research core funding No. P2-0182 entitled Development evaluation).

## 6 REFERENCES

[1] Barimani-Varandi, A., Aghchai, A.J., Lambiase, F. (2021). Failure behavior in electrically-assisted mechanical clinching joints. *Journal of Manufacturing Processes*, vol. 68 p. 1683-1693, **DOI:10.1016/j.jmapro.2021.06.072**.

[2] Mori, K., Abe, Y. (2018). A review on mechanical joining of aluminium and high strength steel sheets by plastic deformation. *International Journal of Lightweight Materials and Manufacture*, vol. 1, no. 1, p. 1-11, **DOI:10.1016/j.ijlmm.2018.02.002**.

[3] Yang, Y., Xiong, X., Chen, J., Peng, X., Chen, D., Pan, F. (2021). Research advances in magnesium and magnesium alloys worldwide in 2020. *Journal of Magnesium and Alloys*, vol. 9, no. 3, p. 705-747, **DOI:10.1016/j.jma.2021.04.001**.

[4] Abe, Y., Kato, T., Mori, K. (2007). Joining of aluminium alloy and mild steel sheets using mechanical clinching. *Material Science Forum*, vol. 561 1043-1046, **DOI:10.4028/www.scientific.net/MSF.561-565.1043**.

[5] He, X., Zhao, L., Yang, H., Xing, B., Wang, Y., Deng, C., Gu, F., Ball, A. (2014). Investigations of strength and energy absorption of clinched joint. *Computational Materials Science*, vol. 94, p. 58-65, **DOI:10.1016/j.commatsci.2014.01.056**.

[6] Maiwald, M., Thiem, J. (2012). Joining without a pilot hole using friction welding. *ATZ Production Worldwide*, vol. 5 10-17, **DOI:10.1365/s38312-012-0045-0**.

[7] Tozaki, Y., Uematsu, Y., Tokaji, K. (2010). A newly developed tool without probe for friction stir spot welding and its performance. *Journal of Materials Processing Technology*, vol. 210, no. 6-7, p. 844-851, **DOI:10.1016/j.jmatprotec.2010.01.015**.

[8] Özdemir, U., Sayer, S., Yeni, Ç. (2012). Effect of pin penetration depth on the mechanical properties of friction stir spot welded aluminium and copper. *Material Testing*, vol. 54, no. 4, p. 233-239, **DOI:10.3139/120.110322**.

[9] Perrett, J.G., Martin, J., Threadgill, P.L., Ahmed, M.M. (2007). Recent Developments in Friction Stir Welding of Thick Section Aluminium Alloys. *6th World Congress, The aluminium Two Thousand*. p. 1-11.

[10] Porcaro, R., Hanssen, A.G., Aalberg, A., Langseth, M. (2004). Joining of aluminium using self-piercing riveting: Testing, modeling and analysis. *International Journal of Crashworthiness*, vol. 9, no. 2, p. 141-154, **DOI:10.1533/ijcr.2004.0279**.

[11] Abe, Y., Kato, T., Mori, K. (2006). Joinability of aluminium alloy and mild steel sheets by self piercing rivet. *Journal of Materials Processing Technology*, vol. 177, no. 1-3, p. 417-421, **DOI:10.1016/j.jmatprotec.2006.04.029**.

[12] Li, D., Chrysanthou, A., Patel, I., Williams, G. (2017). Self-piercing riveting-a review. *The International Journal of Advanced Manufacturing Technology*, vol. 92, p. 1777-1824, **DOI:10.1007/s00170-017-0156-x**.

[13] Di Franco, G., Fratini, L., Pasta, A., Ruisi, V.F. (2013). On the self piercing riveting of aluminium blanks and carbon fibre composite panels. *International Journal of Materials Forming*, vol. 6, p. 137-144, **DOI:10.1007/s12289-011-1067-2**.

[14] Su, Z.-M., Lin, P.-C., Ali, W.-J., Pan, J. (2015). Fatigue analyses of self-piercing rivets and clinch joints in lap-shear specimens of aluminum sheets. *International Journal of Fatigue*, vol. 72, p. 53-65, **DOI:10.1016/j.ijfatigue.2014.09.022**.

[15] Abe, J., Mori, K., Kato,T. (2012). Joining of high strength steel and aluminium alloy sheets by mechanical clinching with dies for control of metal flow. *Journal of Materials Processing Technology*, vol. 212, no. 4, p. 884-889, **DOI:10.1016/j.jmatprotec.2011.11.015**.

[16] Martinsen, K., Hu, S.J., Carlson, B.E. (2015). Joining of dissimilar materials. *CIRP Annals*, vol. 64, no. 2, p. 679-699, **DOI:10.1016/j.cirp.2015.05.006**.

[17] Kaščak, L., Spišak, E. (2013). Mechanical joining methods in car body construction. *Transfer inovacii*, vol. 28, p. 168-171.

[18] Škrlec, A., Klemenc, J. (2017). Parameter identification for a Cowper-Symonds material model using a genetic algorithm combined with a response surface. *Engineering Computations*, vol. 34, no. 3, p. 921-940, **DOI:10.1108/EC-03-2016-0099**.

[19] Bouchard, P.O., Laurent, T., Tollier,L. (2008). Numerical modeling of self-pierce riveting-From riveting process modeling down to structural analysis. *Journal of Materials Processing Technology*, vol. 202, no. 1-3, p. 290-300, **DOI:10.1016/j.jmatprotec.2007.08.077**.

**[20]** Yang, L., Yang, B., Yang, G. W., Xiao, S. N., Zhu, T., Wang, F. (2020). S-N Curve and Quantitative Relationship of Single-Spot and Multi-Spot Weldings. *International Journal of Simulation Modelling*, vol. 3, p. 482-493, **DOI:10.2507/IJSIMM19-3-C011**.

**[21]** Kulawik, A., Wrobel, J. (2020). Numerical Study of Stress Analysis for the Different Widths of Padding Welds. *Strojniški vestnik - Journal of Mechanical Engineering*, vol. 66, p. 567-580, **DOI:10.5545/sv-jme.2020.6771**.

**[22]** Sommer, S., Maier, J. (2011). Failure modeling of a self-piercing riveted joint using LS-DYNA. *8th European LS-DYNA Conference*, Strasbourg.

**[23]** Hanssen, A.G., Oolsson, L., Porcaro, R., Langseth, M. (2010). A large-scale finite element point-connector model for self-piercing rivet connections. *European Journal of Mechanics-A/Solids*, vol. 29, no. 4, p. 484-495, **DOI:10.1016/j.euromechsol.2010.02.010**.

**[24]** DVS/EFB 3480-1:2010 (2010). Testing of Properties of Joints - Testing of Properties of Mechanical and Hybrid Joints. *DVS Media*, Düsseldorf.

**[25]** Wittel, H., Muhs, D., Jannasch, D., Voßiek, J. (2013). *Roloff/Matek Maschinenelemente*, Springer Fachmedien, Wiesbaden, **DOI:10.1007/978-3-658-02327-0**.

**[26]** Škrlec, A., Klemenc, J. (2020). Estimating the strain-rate-dependent parameters of the Johnson-Cook material model using optimisation algorithms combined with a response surface. *Mathematics*, vol. 8, no. 7, p. 1-18, **DOI:10.3390/math8071105**.

**[27]** Wright, A.H. (1991). Genetic Algorithms for Real Parameter Optimization. *Foundations of Genetic Algorithms*, Rawlins, G.J.E. (ed.), vol. 1, Morgan Kaufman, San Mateo, **DOI:10.1016/B978-0-08-050684-5.50016-1**.

**[28]** Temby, L., Vamplew, P., Berry,A. (2005). Accelerating real-valued genetic algorithms using mutation-with-momentum. *The 18th Australian Joint Conference on Artificial Intelligence*, Sydney, p. 1108-1111, **DOI:10.1007/11589990_149**.